PROGRESS REPORT

for the research performed under

NASA Research Grant NAG-1-643

by

Zafer Gürdal

Department of Engineering Science and Mechanics
Virginia Polytechnic Institute and State University
Blacksburg, VA 24061

Table of Contents

Abstract

This report summarizes the progress of the research supported by NASA Grant NAG-1-643. Progress has been made in two areas. One area of research is the failure modelling of anisotropic plates with a through-the-thickness cutout. In the first part of this report an analytical study is presented showing the effects of the notch tip geometry on the location and direction of crack growth from an existing notch in a unidirectional fibrous composite modelled as a homogeneous, anisotropic, elastic material. Anisotropic elasticity and the normal stress ratio theory are used to study crack growth from elliptical notches in unidirectional composites. Sharp cracks, circular holes, and ellipses are studies under far-field tension, and shear loading.

The second area of investigation is to upgrade the capabilities of a previously developed design code to handle more generalized plate geometries and laminates under a more generalized loading and boundary conditions. Discussion of the developments of the design code is presented in the second part.

PART-I: CRACK GROWTH STUDY

Introduction

Understanding of the fracture behavior of notched unidirectional composites can be a building block for the general understanding of the damage growth from existing cutouts and failure of multi-layered composites. Different approaches at both macroscopic and microscopic levels have been used in the literature in order to predict crack growth from existing flaws. Early studies attributed the crack initiation to the shear failure of the matrix along the fiber direction, and the effect of normal stresses perpendicular to the fiber direction is usually neglected. Later investigations, however, revealed that failure initiation and crack growth are governed by the normal stresses in the matrix rather than the shear stresses.

The presents work is an analytical investigation of the influence of initial flaw geometry, fiber orientation, and far-field loading on the location and direction of crack growth in unidirectional composites modelled as homogeneous, anisotropic elastic materials using the Normal Stress criteria.

Crack Growth Predictions

The normal stress ratio (NSR) theory proposed by Buczek and Herakovich [1] is used to predict the location of crack initiation and the growth direction. The theory was originally applied to determine the crack growth direction from a sharp crack embedded in an orthotropic medium. The theory postulates that crack growth will start at the point and extend in a direction, Φ_c, along which the ratio of the tensile stress to strength, both normal to the line of crack growth (Fig. 1a) is maximum. Due to the stress singularity at the tip of a sharp crack the normal stress ratio, R, is calculated at a distance r_0 from the crack tip

$$R(r_0, \Phi) = \frac{\sigma_{\Phi\Phi}(r_0, \Phi)}{T_{\Phi\Phi}}$$

when

$$\sigma_{\Phi\Phi}(r_0, \Phi) > 0$$

The tensile strength, $T_{\Phi\Phi}$ is defined by an elliptical function

$$T_{\Phi\Phi} = X_T \sin^2\beta + Y_T \cos^2\beta$$

where β is the angle from the direction of crack growth to the fiber direction (Fig. 1a) and X_T and Y_T are the longitudinal and transverse tensile strength of the material, respectively. The given form of the strength function satisfies the following necessary conditions,

- For an isotropic material, $T_{\Phi\Phi}$ is direction independent

- For crack growth parallel to the fibers, $T_{\Phi\Phi}$ is equal to Y_T

- For crack growth perpendicular to the fibers, $T_{\Phi\Phi}$ is equal to X_T

The present work extends the application of the normal stress ratio criteria to arbitrary initial flaw geometries ranging from a slit to elliptical cutouts with different aspect ratios including the special case of a circular hole under tensile and shear loads. The approach used provides prediction of the location of the crack initiation as well as the growth direction. Eliminating stress singularities by using a nonzero notch-tip radius, the normal stress ratio can be evaluated at all points around the boundary of a cutout. The geometry for an elliptical flaw and the set of parameters used are shown in Fig. 1b. The location and the direction of crack growth is determined by searching at each point around the notch boundary, $90° \leq \Gamma \leq -90°$, for the direction that maximizes the normal stress ratio. The location of crack initiation is, then, determined to be at the point where the normal stress ratio is the largest for all the points around the notch.

An elasticity solution [2] for the stresses around an elliptical or circular hole is used to determine the location of the point around the notch at which the normal stress ratio predicts crack growth. The solution assumes an infinitely large homogeneous anisotropic plane with a traction free cutout under a remote uniaxial stress, σ^{∞} , applied at an arbitrary orientation from the X axis.

The size and the shape of the cutout is controlled by changing the semiaxes of the ellipse. A special case of a crack can be obtained by setting one of the semiaxes to a zero value. Also by changing

the angle of the applied stress direction various combinations of the normal and shear stresses can be achieved.

Results and Discussion

Crack growth direction and the location of crack initiation are predicted for elliptical notches with different aspect ratios under uniaxial tensile and shear loadings. Stiffness and strength properties typical of a graphite/epoxy, Table 1, are used for material properties. For different notch shapes, the effects of fiber orientation on the normal stress ratio for crack initiation, and on the location and direction of crack growth are evaluated.

Unidirectional Tension:

Elliptical Notch: Predictions are first made for an elliptical notch under a uniaxial stress applied perpendicular to the major axis of the ellipse. The major axis of the ellipse is 2a = 5.08 mm, and the minor axis (2b) is sized so that the radius at the sharp tip is typical of a cut-notch tip radius, r = 0.06 mm. Uniaxial stress of 100 MPa is applied.

Locations and growth directions of cracks emanating from the simulated cut-notch are graphically presented in Fig. 2 for six selected fiber orientations. For all the fiber orientations the crack growth direction is predicted to be along the fiber orientation and the location of crack initiation is related to the fiber orientation. For fiber orientations up to 60°, crack initiation is at a point away from the tip of the ellipse, close to the point where the dashed line crosses the ellipse. The dashed line in the figure represents a typical cut-notch. For fiber orientations larger than 60° the crack initiation is at the tip of the ellipse. High values of the normal stress ratio, associated with high stresses around the cutout, for this relatively sharp elliptical geometry renders the prediction of the failure load with this model.

Stresses around the tip of the cutout become higher as the aspect ratio of the cutout decreases. Such high stresses cause the crack to start from the tip of the ellipse for aspect ratios smaller than 0.05 (essentially a sharp notch) independent of the fiber orientation angle. For such sharp notches the crack growth direction is predicted to be perpendicular to the fibers for the 0° fiber orientation;

however, for all other fiber orientations the crack is predicted to grow parallel to the fibers. Crack growth direction for the 0° orientation proved to be unstable and any slight deviation from the 0° fiber angle resulted in crack growth parallel to the fibers.

Circular Hole: The location of crack initiation and direction of crack growth were predicted for a circular hole under far-field tensile loading. The radius of the hole was equal to the major axis of the ellipse considered above. The effect of fiber orientation on the location of crack initiation and the direction of crack growth can be observed graphically in Fig. 3. The normal stress ratio and the crack growth direction for each of the fiber orientation are plotted as a function of the position angle Γ in Fig. 4.

Trends for the growth direction in Fig. 3 are similar to the previous results for the notch-like elliptical hole except that the growth direction for the 0° fiber orientation is not perpendicular to the fibers but close to the fiber direction itself. The location of crack initiation for the 0° orientation is at a point $\Gamma = 10°$ away from the horizontal axis. Results of recent experimental data for Graphite/Epoxy specimens with a central hole loaded in tension [3] support this finding, Fig. 5. The crack location in Fig. 5 is 13° away from the horizontal axis of the hole. However, figure 4a indicates only a minor difference between the normal stress ratio at $\Gamma = 10°$, where the curve peaks, and at $\Gamma = 0°$ for $\theta = 0°$. Clearly, if the location of crack initiation is at the intersection of the circle with the X axis, $\Gamma = 0$, the crack growth direction would have been predicted to be in a direction ($\Phi = 0°$) perpendicular to the fiber orientation (Fig. 4b).

Elliptical Notch Parallel to the Load: Predictions are also made for an elliptical cutout loaded along the major axis, Figs. 6 and 7. The dimensions of the cutout are the same as the one used before. The results in Fig. 6 show that the point of crack initiation is a strong function of fiber orientation. The crack is predicted to grow parallel to the fibers in all cases considered except for $\theta = 0$. Figure 7 shows that both the value of the NSR and the predicted crack growth direction are very weak functions of the position angle. Although for each fiber orientation there is a peak value of the normal stress ratio (Fig. 7a), the flatness of the curves (especially the curves for the 0° and the 90° fiber orientations) suggest that the crack initiation is possible over a wide range of the position angle Γ without a significant change in the stress level that causes crack initiation.

Although the crack growth direction predictions (Fig. 7b) are consistently along the fiber direction for almost the entire range of the position angle for the 90° and other off-axis angles, the crack growth direction changes significantly for the 0° orientation. It ranges from $\Phi = 90°$ (along the fiber direction) if the crack is located close to the sharp tip of the ellipse to $\Phi = 0°$ (perpendicular to the fiber direction) if the crack is located at the horizontal axis along the edge. The low values of the normal stress ratio for 0° fiber orientation indicates the insignificance of a long slender notch parallel to the fibers on the stresses around the notch.

The normal stress ratios for three fiber orientations, 0° 45° and 90°, are plotted in Fig. 8 as a function of the logarithm of the cutout aspect ratio b/a. Each curve is normalized with respect to the normal stress ratio of the circular hole of corresponding fiber orientation. As the notch becomes more crack-like (smaller b/a) the normal stress ratio increases rapidly. The gradient is higher for a 0° fiber orientation compared to the 45° and 90° orientations. This figure clearly shows the influence of flaw shape and fiber orientation on the fracture behavior of unidirectional composites. It is interesting to note that similar predictions for an isotropic material are obtained to be almost identical with the curve for the 90° fiber orientation.

In-plane Shear:

For the same notch geometries considered under tensile loadings, the crack location and growth direction predictions are obtained under pure in-plane shearing load of 100 MPa. The predictions for the off-axis fiber orientations are made for both positive and negative values of the loading since the direction of the applied shear effects the normal stress ratio, and the crack growth direction.

Elliptical Notch: For the simulated notch, predictions of crack growth direction and location are presented in Fig. 9. Since the analytical solution used for the stresses is based on infinite plate assumption, predictions for a vertical notch coincides with the predictions of the horizontal notch and, therefore, are not repeated. However, in a real experimental test coupon the finite size of the test specimen can be expected to change this behavior. Investigation of the finite size effects of the specimen on crack growth is not considered during the present work.

The location of crack growth in Fig. 9a for the 0° fiber orientation agrees with the experimentally observed crack location in Iosipescu shear test specimens of reference [4]. The amount of off-set of the crack location from the tip of the notch is more pronounced for all the shear loading cases compared to the uniaxially tension loaded fiber orientations. Even for the 90° fiber orientation, the crack location is slightly away from the crack tip location, Fig. 9b. For all fiber orientations, the predicted directions of crack growth were along the fiber direction. However, as indicated in Figs. 9c - 9h, the location of crack growth changes symmetrically about the horizontal axis when the sign of the shear stress is reversed.

Circular Hole: The locations and the crack growth directions are graphically presented in Fig. 10 for circular holes with various fiber orientations under pure shear loading. For the 0° orientation, Fig. 10a, the location of the crack is predicted to be as much as 55 degrees away from the horizontal axis. As the fiber orientation is increased, the location of the crack moves closer to the horizontal axis for both positive and negative shear loadings.

Following the previous results, crack growth directions from the circular hole were along the fiber direction, except for the 45° orientation under positive shearing load. For that particular loading and fiber orientation, the crack is predicted to propagate in a direction perpendicular to the fiber orientation, therefore, causing fiber failures. Plots of the normal stress ratio and crack growth direction at each point around the hole in Fig. 11, however, indicates that for the 45° orientation under positive shear the normal stress ratio levels-off around the peak value suggesting adjacent points with equal likelihood of crack initiation. Clearly, the crack growth direction plot (Fig. 11b) indicates that, if the crack initiation is not right at 45°, the crack will grow in a direction close to the fiber direction (close to either +45 or -135 degrees).

Finally, it is clear from Fig. 11 that the load level at which the normal stress ratio predicts crack initiation for off-axis orientations is strongly influenced by the direction of the applied shear. For the 0° and the 90° orientations, the same maximum value of the normal stress ratio is achieved under a positive or negative 100 MPa shear loading. For the 45° orientation, on the other hand, the critical normal stress ratio under the negative shear is 8.5 times the critical normal stress ratio under the positive shear. This result suggests that the crack initiation load of the 45° orientation under positive shear is 8.5 times larger than the negative shear loading.

Concluding remarks

Results of this study have indicated that the location of crack initiation depends on the shape of the initial flaw, the degree of material orthotropy with respect to the loading direction, and the direction of applied stresses. For very sharp notches under unidirectional tensile loading, crack initiation is predicted to be at the notch tip. For elliptical and circular cutouts the location of crack initiation is a strong function of the orientation of the fibers with respect to the loading direction. Under normal stresses applied perpendicular to the major axis of the ellipse, crack initiation is at the tip of the ellipse for fiber orientations larger than 60°. For all other fiber orientations the crack initiation is at the edge of the ellipse away from the tip. For most of the cases investigated, the crack growth direction is predicted to be along the fiber direction.

The effects of notch geometry and fiber orientation on crack location are more pronounced for pure shear loading. For a circular hole with 0° fiber orientation, the location of the crack initiation is at a point 55 degrees from the horizontal line perpendicular to the fibers. Also, the normal stress ratio at crack initiation proved to be a strong function of the direction of the applied shearing load.

The material discussed in this part has been accepted for publication in the Journal of Theoretical and Applied Fracture Mechanics. Application of the model to predict crack growth under compressive loads is presently under consideration.

References

[1] Buczek, M. B., and Herakovich, C. T., "A Normal Stress Criterion for Crack Extension Direction in Orthotropic Composite Materials," **"J. of Composite Materials,"** Vol. 19, Nov. 1985, pp. 544-553.

[2] Savin, G. N., **"Stress Concentrations around Holes,"** Pergamon press, Oxford, 1961.

[3] Post, D., and Czarnek, R., Private communications, Engineering Science and Mechanics Department, Virginia Polytechnic Institute and State University, Nov. 1986.

[4] Beuth, J. L., Jr., Gürdal, Z., and Herakovich, C. T., "Composite Fracture Using the Normal Stress Ratio Theory", **Symposium on Advances in Composite Materials and Structures**, (S. S. Wang, ed) ASME Winter Annual Meeting, Anaheim, CA, December 1986.

Table 1: Unidirectional material properties used.

Longitudinal Modulus, E_1	10.20 MSI
Transverse Modulus, E_2	1.56 MSI
Shear Modulus, G_{12}	0.82 MSI
Major Poisson's Ratio ν_{12}	0.24
Longitudinal Tensile Strength, X_T	219.50 KSI
Longitudinal Compressive Strength, X_C	-246.00 KSI
Transverse Tensile Strength, Y_T	6.35 KSI
Transverse Compressive Strength, Y_C	-23.80 KSI
In-plane Shear Strength, S	12.60 KSI

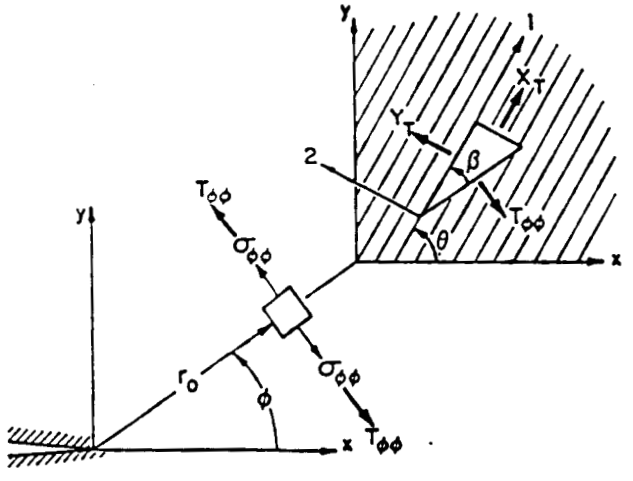

a) for a crack.

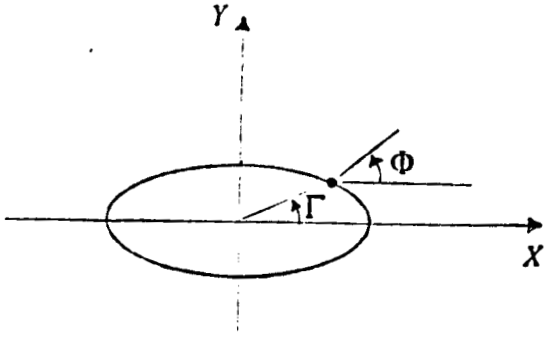

b) for an elliptical cutout.

Figure 1: Normal stress ratio parameters.

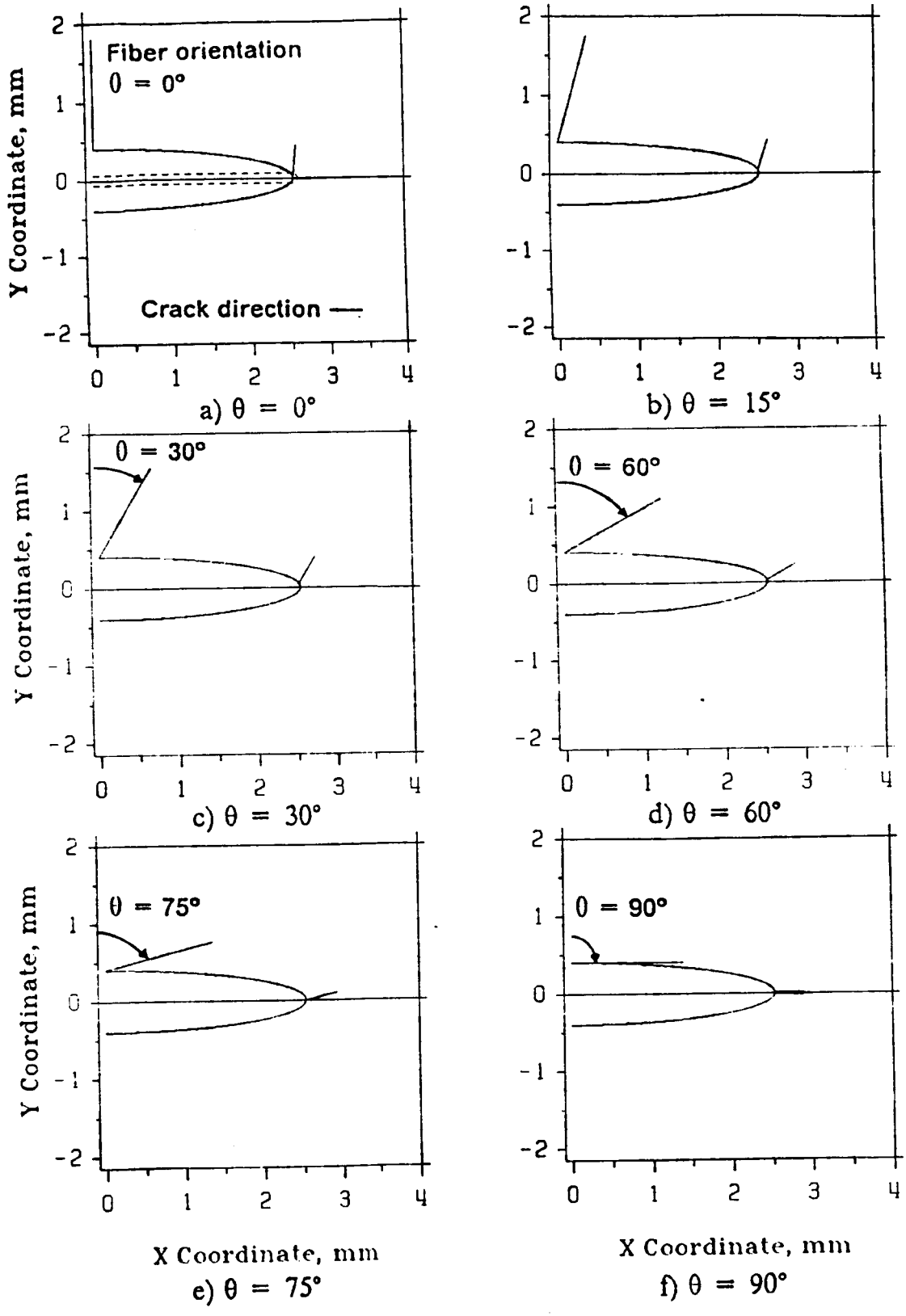

Figure 2: Crack growth from an elliptical cutout under a normal stress applied perpendicular to the major axis (b/a = 0.158).

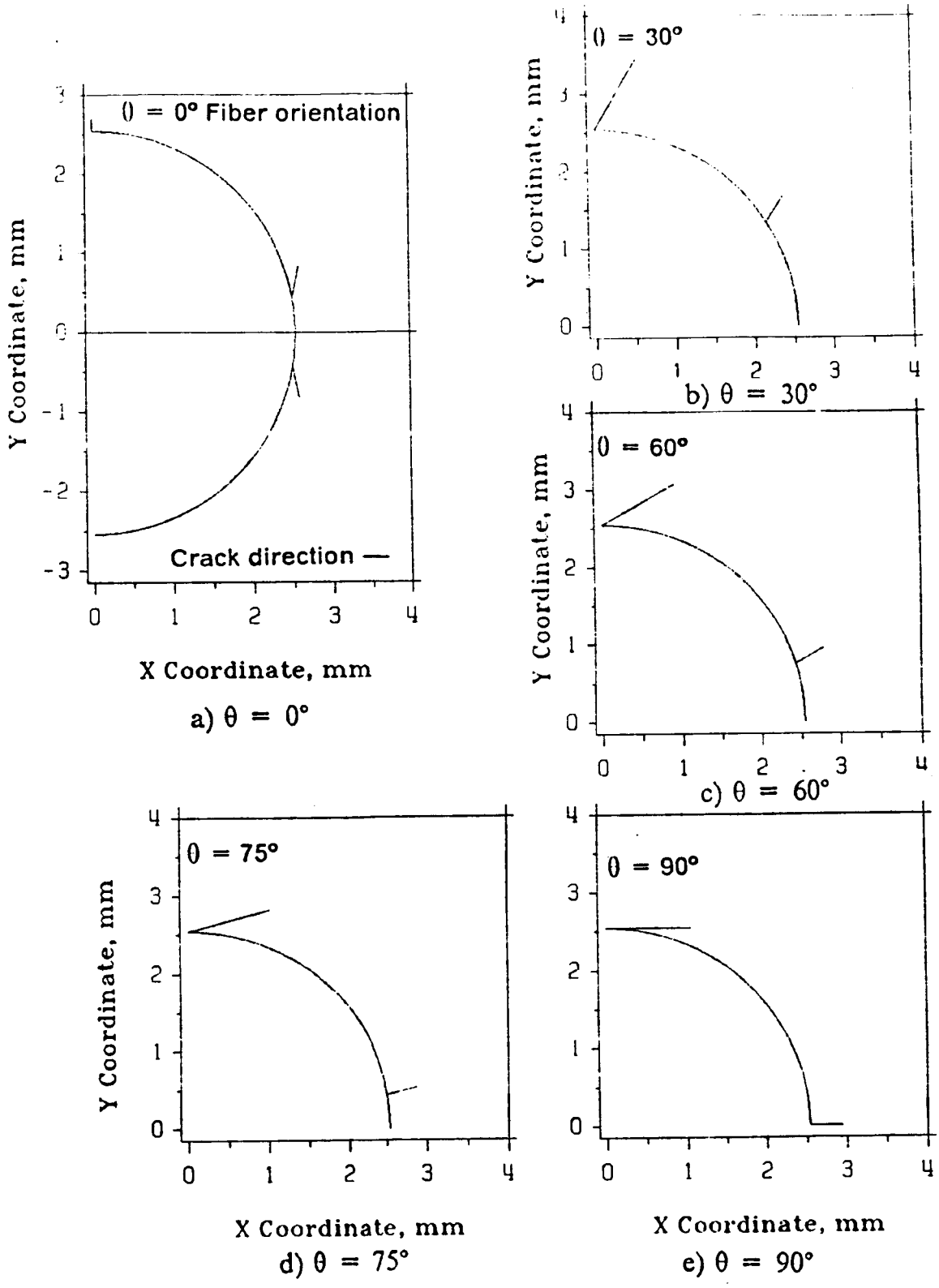

Figure 3: Crack growth from a circular cutout under a normal stress.

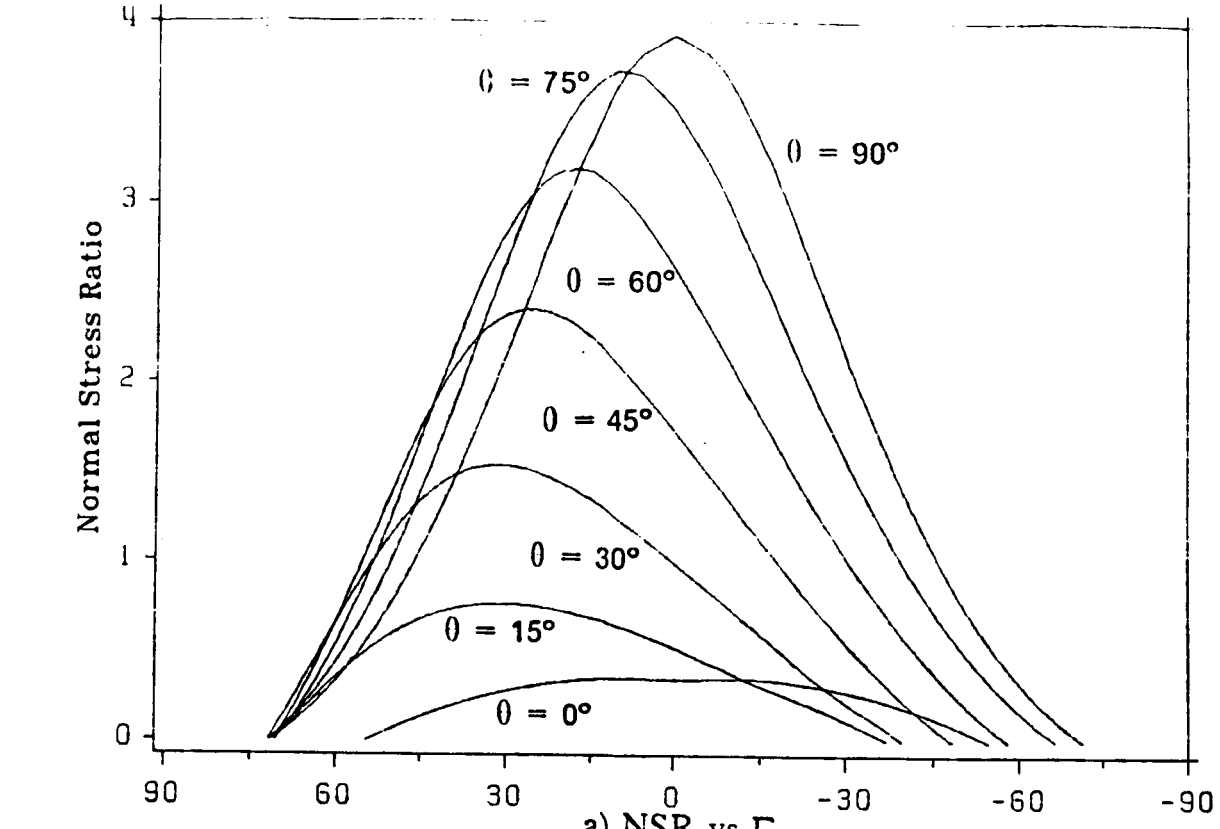

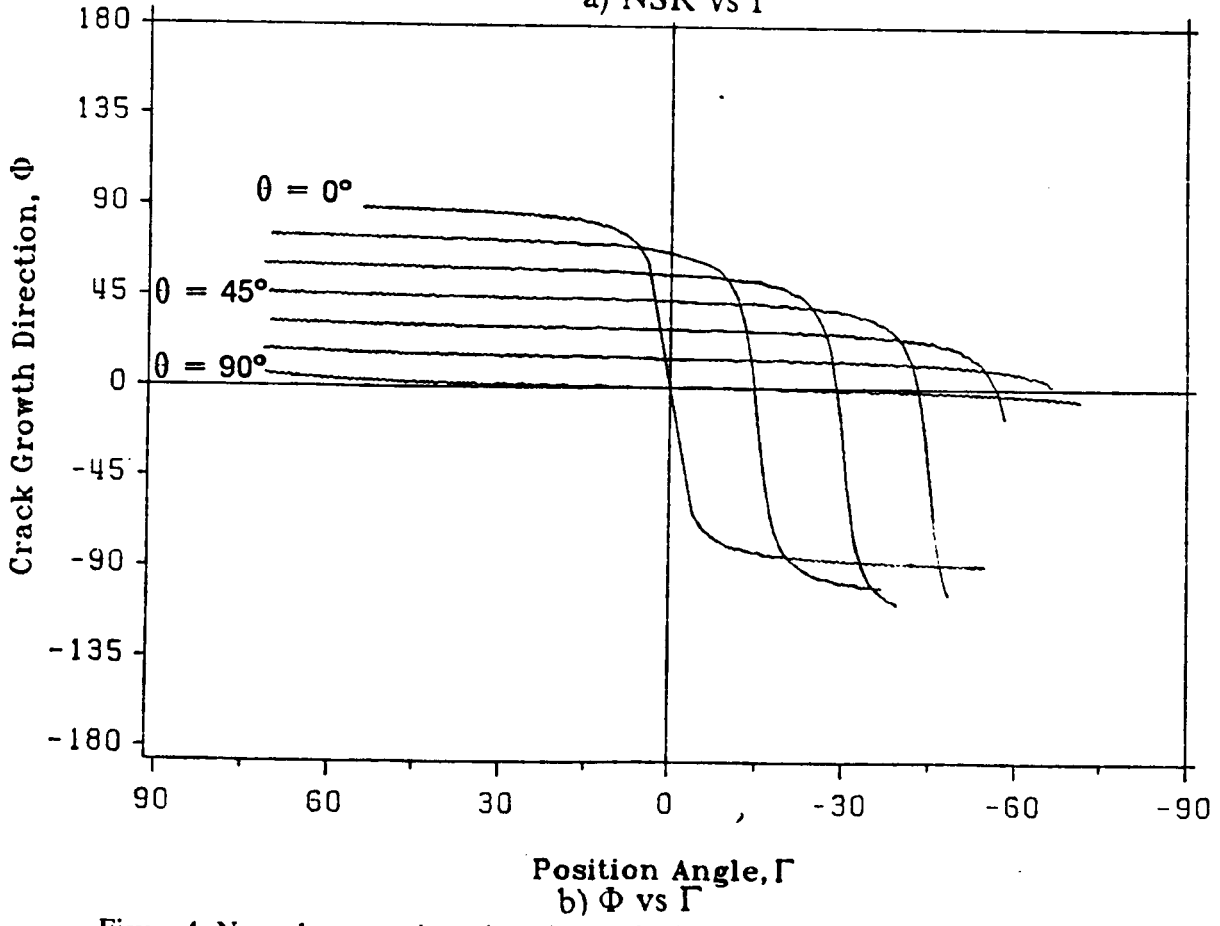

Figure 4: Normal stress ratio and crack growth direction around a circular cutout under a normal stress.

ORIGINAL PAGE IS
OF POOR QUALITY

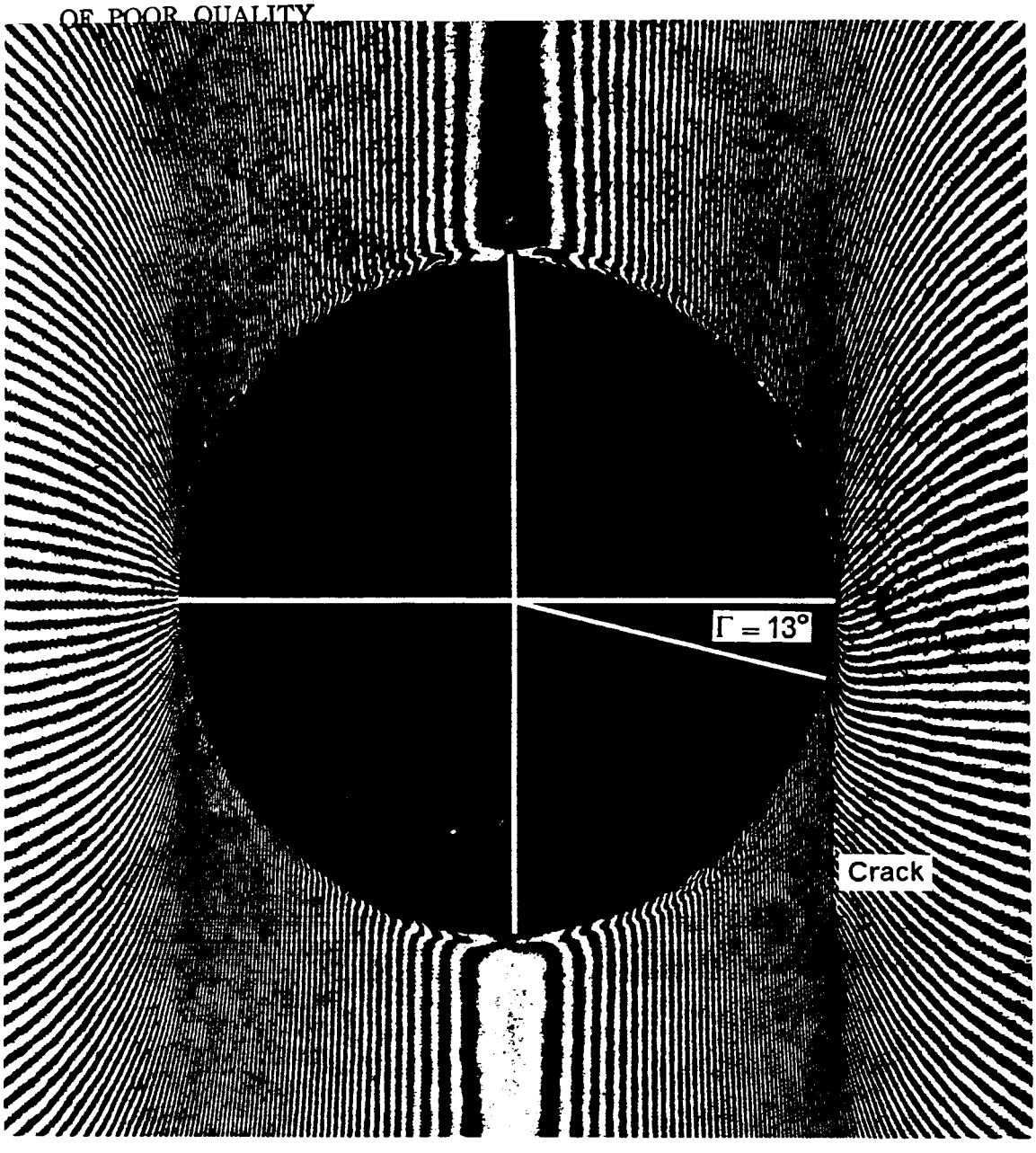

Figure 5: Crack growth from a circular cutout under a normal stress.

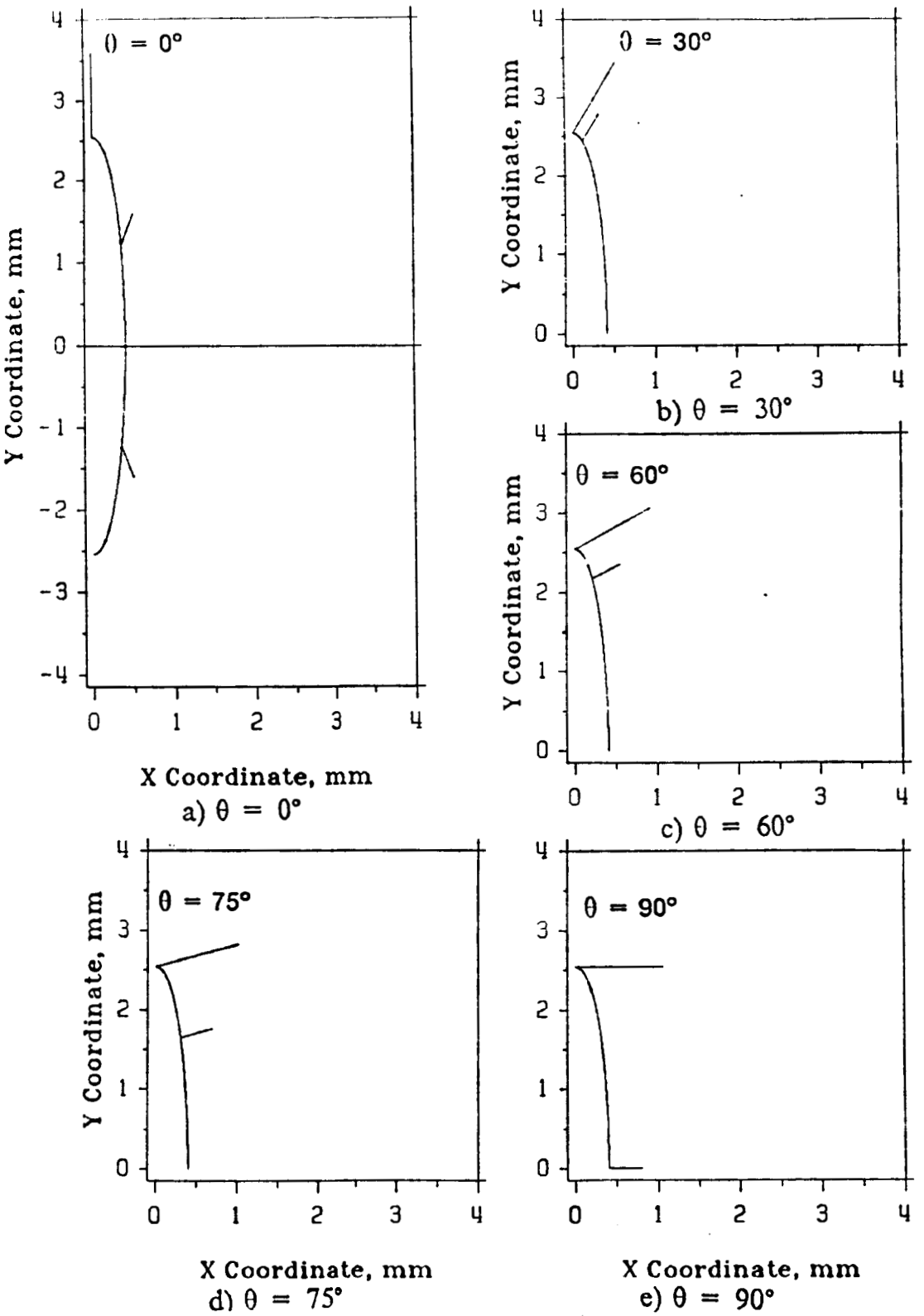

Figure 6: Crack growth from an elliptical cutout under a normal stress applied parallel to the major axis (b/a = 6.35).

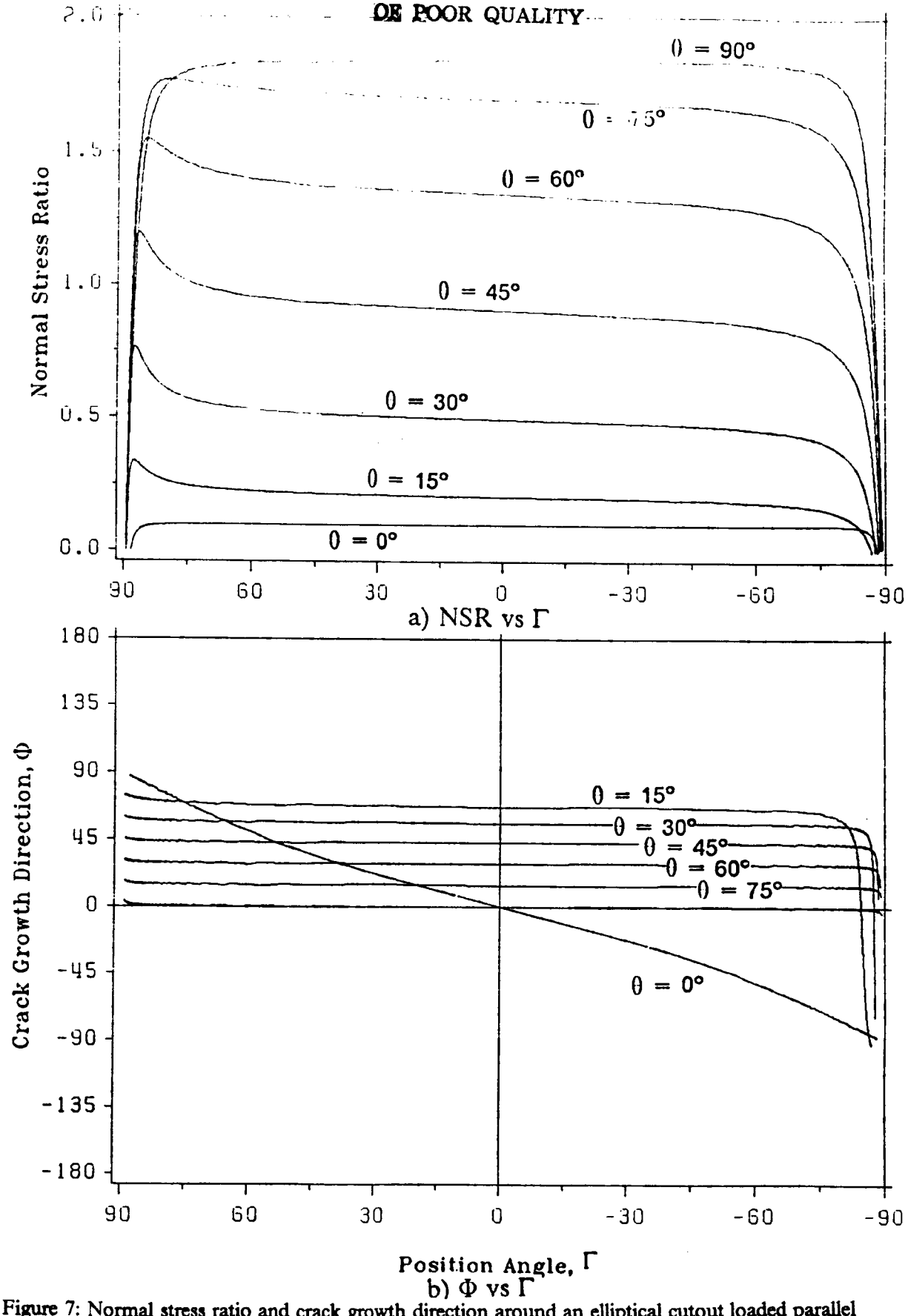

Figure 7: Normal stress ratio and crack growth direction around an elliptical cutout loaded parallel to the major axis (b/a = 6.35).

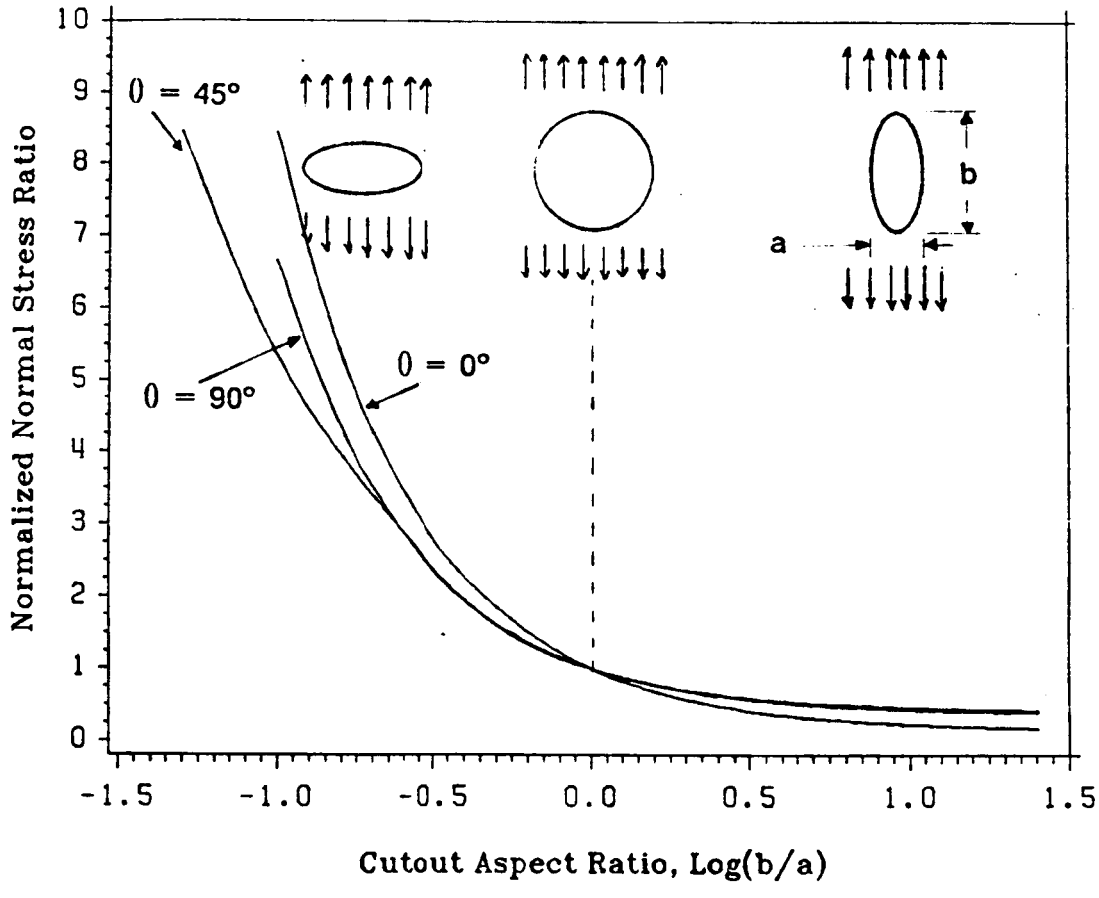

Figure 8: Normal stress ratio (normalized with respect to the normal stress ratio of a circular hole) as a function of cutout geometry.

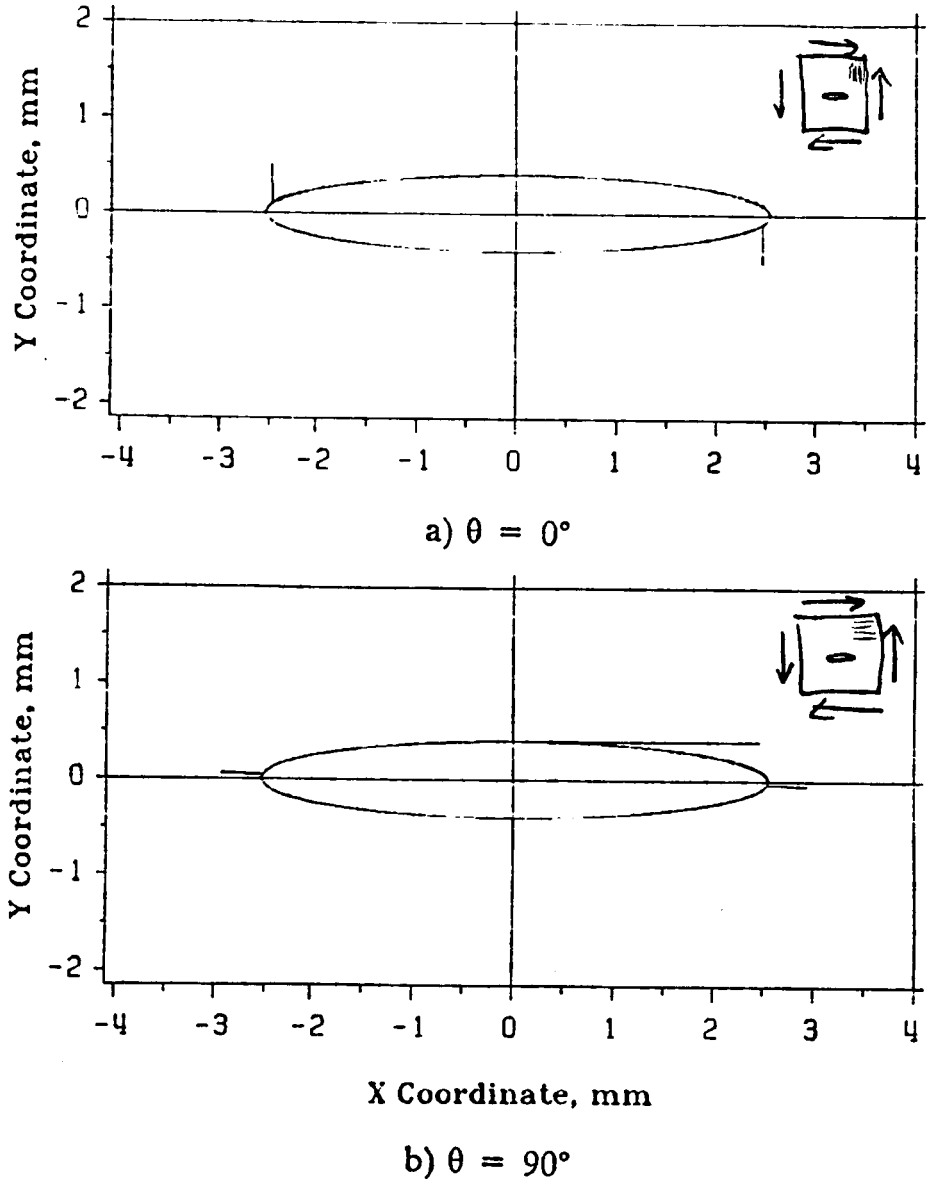

Figure 9: Crack growth from an elliptical cutout under pure shearing stress (b/a = 0.158).

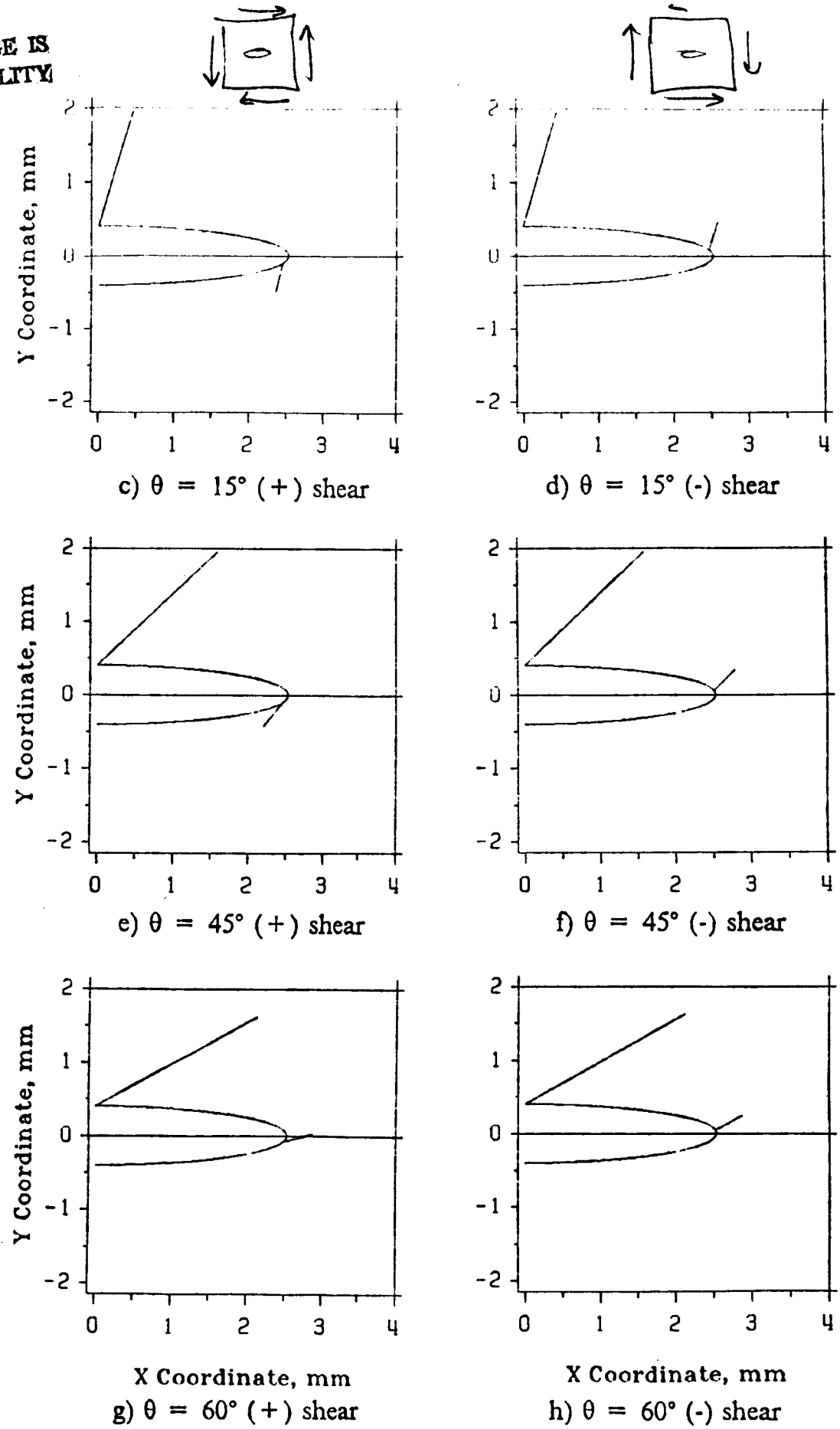

Figure 9: Continued

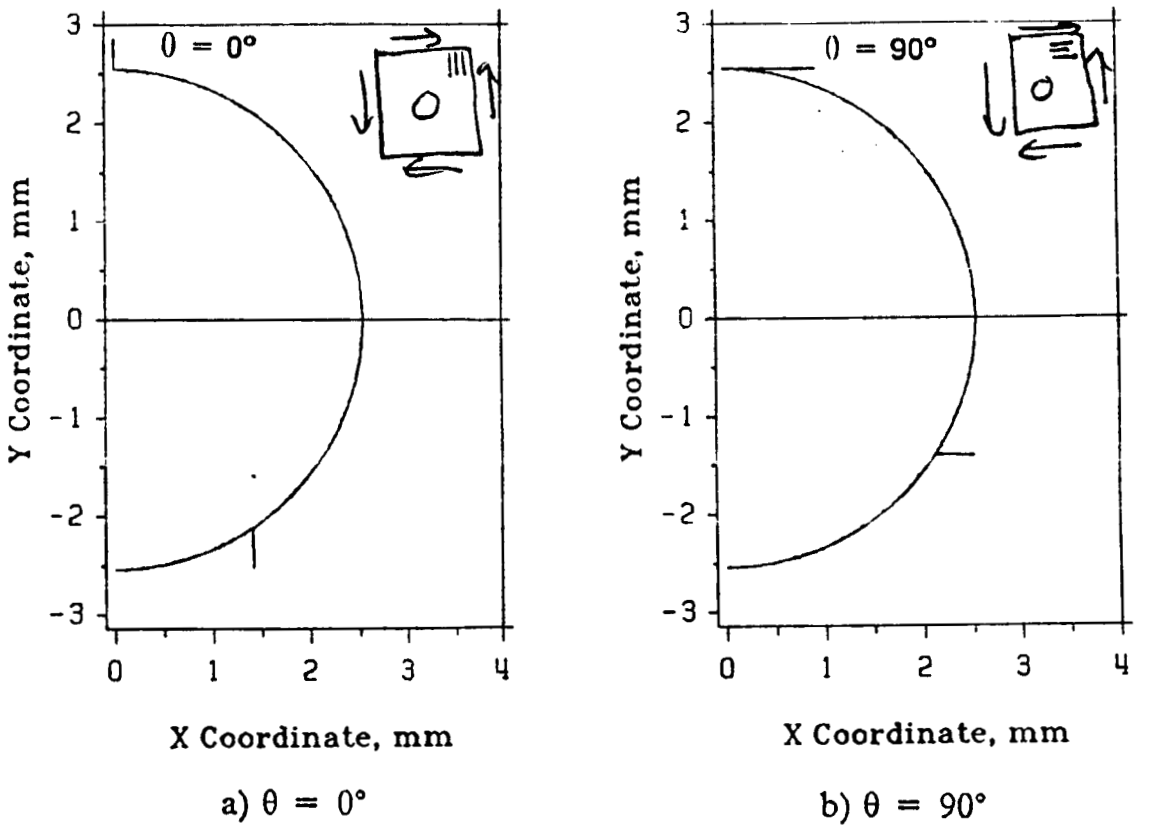

a) θ = 0°

b) θ = 90°

Figure 10: Crack growth from a circular cutout under pure shearing stress.

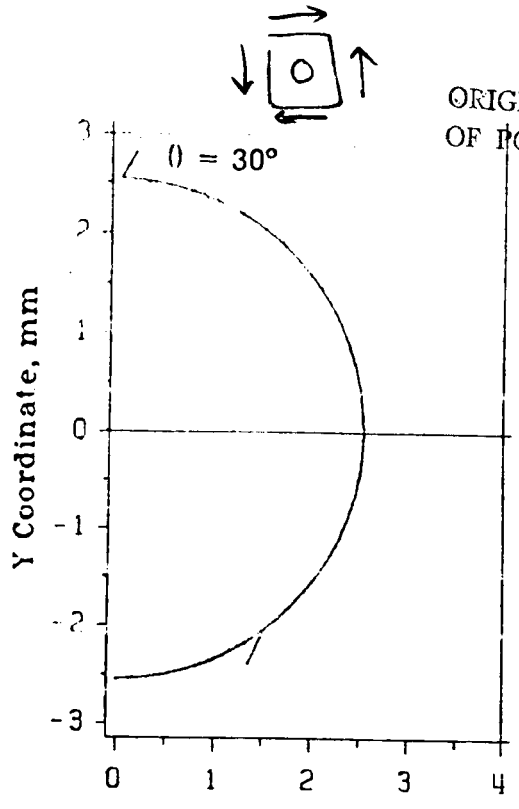

c) θ = 30° (+) shear

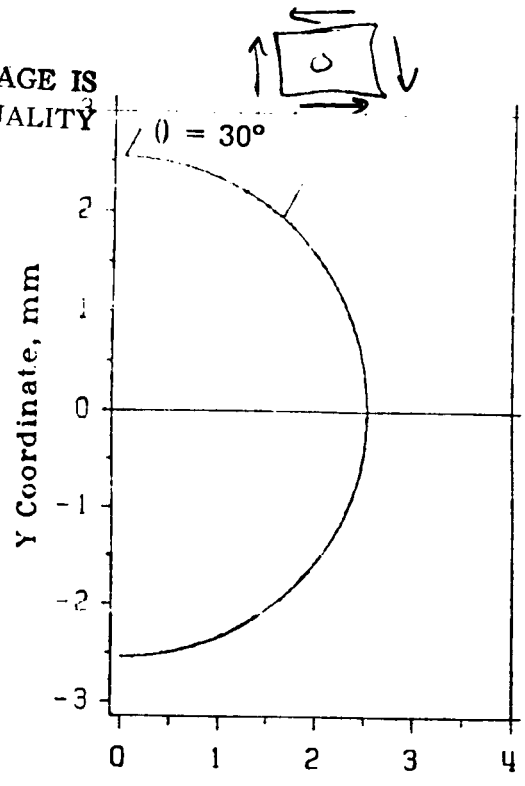

d) θ = 30° (-) shear

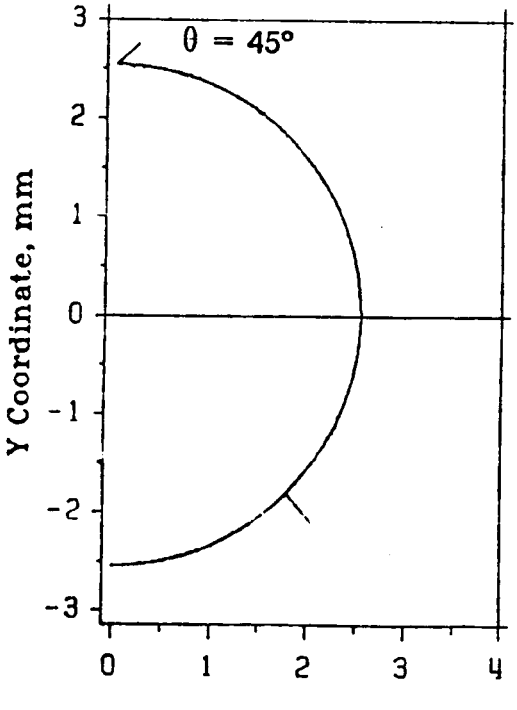

e) θ = 45° (+) shear

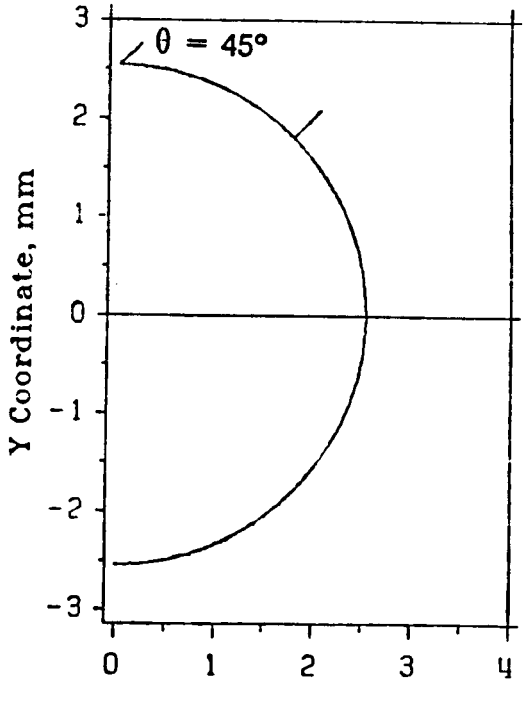

f) θ = 45° (-) shear

Figure 10: Continued

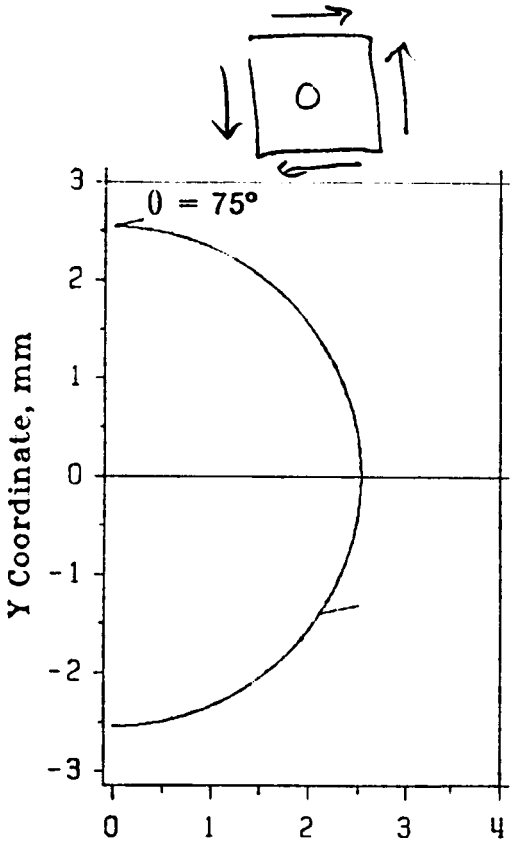

g) θ = 75° (+) shear

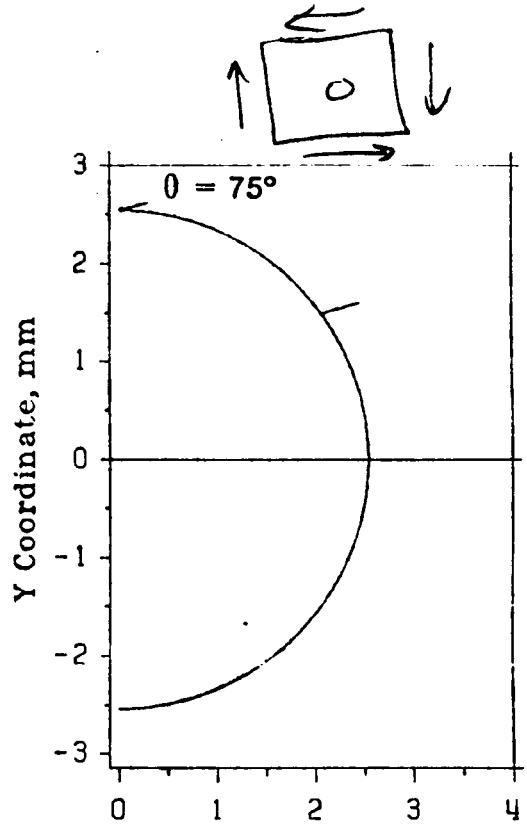

h) θ = 75° (-) shear

Figure 10: Continued

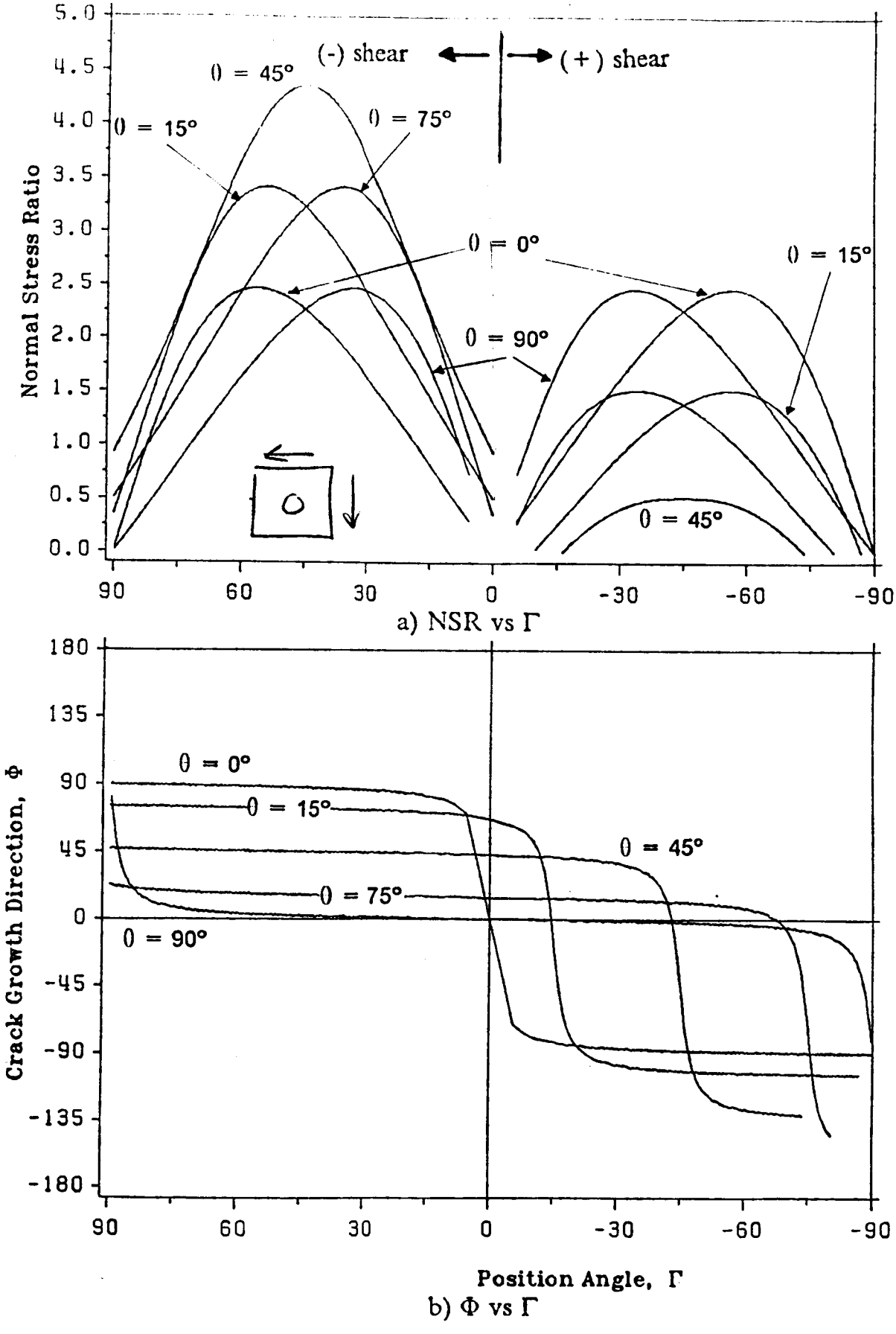

Figure 11: Normal stress ratio and crack growth direction around a circular cutout under shearing stress.

PART-II: MODIFICATION OF THE DESIGN CODE

Introduction

In a recent study [1] an optimization procedure for designing stiffened and unstiffened orthotropic plates is used to achieve minimum weight plate configurations that are resistant to damage growth. The design code used in reference [1] is developed by integrating the finite element analysis program of reference [2] with an optimization package [3]. A special mesh generation program is used to interface the two programs. The mesh generator is limited to only rectangular symmetric unstiffened plates, and symmetric stiffened plates with constant cross-section stiffeners along the length of the plate. Only orthotropic laminates loaded along the principal axis of orthotropy are considered. Although the above assumptions resulted in significant computational cost savings associated with a simpler finite element modelling of the plate with a minimum effort, plate structures used in aircraft are not symmetric and are usually under the application of a combination of in-plane loads. Also transverse stiffeners or stiffeners that form grid patterns are common forms of reinforcing structures. This part of the report deals with upgrading our analysis and design capabilities to include more generalized plate geometries, laminates, loading and boundary conditions. With the proposed modifications, it will be possible to investigate the efficiency of various advanced design concepts and configurations under different loading and damage conditions.

Program Modifications

The approach for modifying the design code to handle more general plate geometries is to use the mesh generation capabilities of the original finite element program [2]. That is, for a given plate configuration the designer has to decide the finite element modelling of the geometry. This includes deciding the number of elements to be used, the node point locations, restrain specifications, and defining the loads or displacements to be applied to the model. Once the model topology is defined, material properties, stacking sequence, and thicknesses of different sublaminates that will be used to construct the different sections of the plate structure is defined. Since the finite element analysis used is a membrane analysis, only one layer of elements in the

thickness direction is used. Therefore, the sections of the plate with different thicknesses, such as stiffeners, are obtained by assembling sublaminates to form the laminate of the desired section and assigning these smeared properties to the appropriate elements within that section. Finally, from the various thicknesses and ply orientations that are used as input to the program, those variables which will be used as design variables are identified.

Portions of a typical input data for a rectangular unstiffened plate are shown in Table 1. Purpose of each of the cards, or group of cards, are marked on the table, and discussion of some of the features of the input data shown in Table 1 is presented in the following section. Although, the input requirements for the mesh generation of the finite element program is rather complicated and time consuming, once the mesh for the initial geometry is generated, it will be used for the rest of the design process provided that the geometry of the plate will remain the same. The author is in the process of modifying the users manual of the previous design code [1] to include the new capabilities, and the manual will soon be made available.

Input Data Organization

Functions of the different portions of the input data are explained in this section. Note that the lines with an only 0 entry indicate the end of a specific portion of the data.

The first line in the input data shown in Table 1 is used to specify whether the run is an design optimization or an analysis run, and select the automatic or manual mesh generation option. Following the second line which is the title of the run, the numbers of nodes, elements, cracked elements, restrained nodes, nodes with applied forces or displacements, and number of material code numbers in the model are defined in the third line.

The next group of lines specify the node point coordinates in the model. Besides specifying the location of a node, it is also possible to increment the node number(s) and coordinates of a single or group of nodes to generate additional nodes (node point bumping) with minimum number of input lines. Following the node point coordinates, nodes or a group of nodes to be restrained in certain directions are specified. The bumping feature can also be used for restraint definitions of more than one node.

The next data group specify the triangular element topology data. Similar to the node point data, bumping feature can be used to specify the connectivities of a group of elements as well as single elements. Next the element material code definition data, which associates certain elements with appropriate smeared material properties, is provided. The material code numbers refer to different combinations of sublaminates that will form the thickness of a given section of the plate. The definitions of the material code numbers are provided later in the input sequence after the sublaminate definitions. In the sample input data shown in Table 1, all the elements are assigned to have the same material code number. In a more general case it is possible to specify different material code numbers for the elements at different sections of the plate that will confirm with the geometry of the plate.

Following the material code number definitions, is the line that define the direction of the material reference axis which is taken from the first node to the second node specified in that line. All the ply orientations specified in the following lines for sublaminate definitions refer to this direction.

The sublaminate definitions start with the material properties specified in the first line of that group. The second line of the group indicates the number of plies with different orientations in that sublaminate. In the third line thicknesses, and in the fourth line orientations of each of the layers are specified. It is also possible to assume each sublaminate to be a single layer with one orientation only, as indicated in the table as an alternate definition. This feature makes it possible to even specify different material properties to different ply orientations and, therefore, construct hybrid laminates. The material code definitions for these two alternate ways of input are slightly different, and both indicated in the table. Following the material code number, the second number in the first line of that group indicates the number of sublaminates that make up the laminate for that material code number. The second line of that group specifies the sublaminate numbers that are used for that material code number. The number of entries in this line must be equal to the second number in the first line. Note that the alternate material code definition uses all three sublaminates to form the same laminate which is defined by a single sublaminate in the original data sequence.

If a crack is included in the analysis or design of the plate, then the model includes either 8-noded or 10-noded crack-tip elements which are defined by the node points of the elements. The material code number which will be used for that element is also included in the same line that define the crack-tip element. The input data given in Table 1 include only one 8-noded crack-tip element.

The loading definition is made in the next group of data. It is possible to specify either the displacement or the force acting at selected nodes of the mesh along the x or y coordinate axis.

Finally information related to the design portion of the input is needed. The first line of this portion of the data indicates the number of design variables, number of total constraints, and the number of user defined constraints. The number of entries in the second line is equal to the number of design variables, and indicate whether lower, upper, or a combination of lower and upper bounds used on the design variables. Regardless of the type of bounds specified in this line, the next two lines specify the possible upper and lower bound values for each of the design variables. And finally the last line indicates the selection of the design variables from the list of thicknesses and orientations input earlier during the sublaminate definitions. The value of the thickness of each ply is stored in an array following the same input sequence followed by the orientations of those plies. The numbers in this last line refer to the locations of the variables in that array which will be used as design variables.

Stress Constraints

An additional feature has been incorporated into the design code to implement a stress failure criterion at various locations in the plate. Previously [1], the stress constraints applied to the problem were calculated based on average stresses calculated from the loads applied to the undamaged plate. That is, local stress concentrations (except the crack-tip stress singularity which is taken into account by another constraint) has been neglected and the rectangular plate is assumed to have uniform stresses distribution along the length. With the modifications made to the program, it is possible to design complicated geometries which can potentially introduce localized stress concentrations that need to be monitored during the design process. The failure

criterion used allows the option of performing a Tsai-Wu failure analysis of the selected elements of the finite element mesh based on the stresses obtained from the finite element stress analysis. Although it is possible to implement the failure analysis for each of the elements in the mesh, this would result in an prohibitively expensive design optimization run. Instead, it is recommended that the most stress critical elements of the different regions of the plate which are governed by different design variables be selected and the stress constraints applied at those selected elements of the mesh.

Applications

Beside allowing anisotropic laminates of arbitrary shapes under general in-plane loadings, the modified design code allows designing plates with different crack locations and orientations, as opposed to the previous code in which only a central crack located normal to the applied load is possible. It is also be possible to design plates which have different thicknesses at different sections even along the length of the plate. This feature is particularly important since it enables the designer to consider new structural concepts and design configurations. The damage tolerance constraint build into the design code will also enable the designer to evaluate the response of different design configurations to a damage condition.

In order to demonstrate the application of this program to new design concepts, two structural configurations for stiffened plates are studied to quantitatively evaluate the effects of stiffener thickness variation on stiffness, strength, and damage tolerance. The two configurations are essentially grid-stiffened configurations, one with a rectangular pattern of stiffeners (generally referred to as an orthogrid plate), and the other one with stiffeners forming equilateral triangular shapes (commonly known as an isogrid plate configuration). The plates are loaded by axial normal, shear, and combinations of axial and shear stresses to cover a wide range of load applications.

A finite element mesh is generated for each plate configuration, using triangular elements to define the plate and stiffener geometries, Fig. 1. The plate configurations are selected in such a way that both had an equal number of vertical (or close to vertical) stiffeners and the plate sizes

were same. The orthogrid configuration has four longitudinal and five transverse stiffeners, all with a unit width (Fig. 1-a). The isogrid configuration has stiffeners of unit width oriented at plus and minus 30 degrees with respect to the longitudinal axis. Together with the four transverse stiffeners they create a series of equilateral triangles which form the grid-stiffening structure (Fig. 1-b).

The thickness or depth of the stiffeners is the primary variable in this study. The stiffener thickness represents the total thickness of stiffener material added to the surface of a quasi-isotropic skin. The skin thickness is assumed to be constant and equal to 0.1 inches. At the node points of the grid-structure where two stiffeners intersect the total thickness of the stiffener is twice the thickness of stiffener material.

Both plates are subjected to a uniform unit longitudinal displacement along the loaded edges. The overall stiffness and the strength of these configurations are determined as the stiffener thickness is increased. Also, effects of local damage on the stiffness and strength are investigated. To determine the response of these two plate configurations to a local damage, material properties of a group of elements in the skin panel are set equal to zero. These results are compared to the data gathered on the undamaged plates. For example, typical stiffness to weight plots as a function of the stiffener thickness for the orthogrid and isogrid configurations are presented in Figs. 2 and 3, respectively. The solid lines in the figures represent the undamaged plates, and the dashed lines are for the plates with an opening in one of their skin panels. For the orthogrid configuration, as the relative thickness of the stiffener with respect to the skin thickness in increased the specific stiffness of the plate increases. However, for the isogrid configuration, the situation is reversed and the effective stiffness seem to reduce slightly. This is thought to be the result of reduced skin effectiveness in preventing the scissoring action of the triangular stiffeners under applied longitudinal displacements. Local skin panel damage seems to somewhat reduce the specific stiffness of both plate configurations for low values of the stiffener thickness. For plates with thick stiffeners the effect of the opening on stiffness vanishes. Also, the effect of the local opening, although small for both plate configurations, seems to be more pronounced for the isogrid plate configuration. For example, for a stiffener thickness of 0.3 inches the reduction in specific stiffness is about 5% for the isogrid plate compared to 2% for the orthogrid plate. In order to achieve a better understanding of the two

design configurations, other structural responses under variety of loading conditions must be evaluated and the effects of number of geometric and material parameters must be investigated. Currently, the author is in the process of evaluating such configurations to design an optimum grid stiffened plate for aircraft applications.

Concluding Remarks

The previously developed design code for damage tolerant plates has been modified so that user defined meshes can be used to model stiffened and unstiffened plates with complex geometries under combined in-plane loadings. The main advantage of this modification is the possibility of extending our design capabilities to new structural configurations, and investigating the damage tolerance of such configurations. Design of complicated configurations also require more stringent control of the local stress concentrations during the design. A subroutine for failure analysis based on exact finite element stress resultants of the design code has been added to the procedure so that strength constraints at any point in the plate can be imposed. The program is then used to investigate the effects of ply thicknesses on stiffness, strength, and the damage tolerance of two grid-stiffened plate configurations.

References

[1] Gürdal Z., and Haftka R. T., "Automated Design of Composite Plates for Improved Damage Tolerance," **ASTM Composite Materials Testing and Design: Eighth Symposium**, April 27, 1986.

[2] Chu C.S., Anderson J.M., Batdorf W.J., Aberson J.A., Simpson K.M., "Finite Element Computer Program to Analyze Cracked Orthotropic Sheets," NASA CR-2698, July, 1976.

[3] Grandhi, R. V., Thareja, R. R., and Haftka, R. T., "NEWSUMT-A: A General Purpose Program for Constrained Optimization using Constraint Approximations," **ASME Journal of Mechanisms, Transmissions, and Automation in Design**, Vol. 107, March 1985, pp. 94-99.

Table 1: A typical input data for the design code

```
================================================================
 0  0
A TYPICAL MESH FOR THE DESIGN AND ANALYSIS OF AN UNSTIFFENED PLATE
157 254  1  0  0  32  2  1  1  11
 1  0.0        0.0
-1  0.0        2.333625   5  1  1
-1  0.0        2.381250   3  1  1
-1  0.0        2.411016   8  1  1
18  2.381250   0.0                    -> NODE POINT COORDINATES OF THE F.E. MESH
-1  0.0        2.349500   4  1  1
         .           .
         .           .
123 48.815625  0.0
-1  0.0        9.525000   4  1  1
-1  10.914062  0.0        6  5  5
 0
 1   0   1   3   17
     .       .                        -> NODAL RESTRAINT DEFINITIONS
     .       .
154  -1   0   3   1
 0
 1   1   2   18
 2   2   19  18                       -> TRIANGULAR ELEMENT DEFINITIONS
-1   1   1   1   4   2   2
         .           .
         .           .
207  123  124  128
208  124  129  128
-1   1   1   1   3   2   2
-1   5   5   5   5   8   8
 0
 1   1  253   1 -> ELEMENT MATERIAL CODE DEFINITION
 0
 1  18 -> DIRECTION OF MATERIAL AXIS
 1  2  131.0E3  13.00E3  6.4E3  0.3800     <->   ALTERNATE SUBLAMINATE DEFINITION.
 3                                               1  2  131.0E3  13.00E3  6.4E3  0.3800
  2.24     1.12     0.56                         1
  0.0      45.0     90.0                          2.24
 0                                                0.0
 1  1                                            2  2  131.0E3  13.00E3  6.4E3  0.3800
 1                                               1
 0                                                1.12
 1  9  26  25  24  23  6  7  8  1                 45.0
 0                                               3  2  131.0E3  13.00E3  6.4E3  0.3800
 1     -122000.0                                 1
153     0.1000   0.0                              0.56
  .       .                                       90.0
  .       .           -> LOADING DEFINITION
157     0.1000   0.0                             1  3
 0                                               1  2  3
 3  0  0                                         ALTERNATE MATERIAL CODE NUMBER DEFINITION
 1  1  1
  0.28      0.28      0.28
 1.0E+10   1.0E+10   1.0E+10   LOWER AND UPPER BOUNDS ON DESIGN VARIABLES
 1  2  3 -> DESIGN VARIABLE DEFINITIONS.
================================================================
```

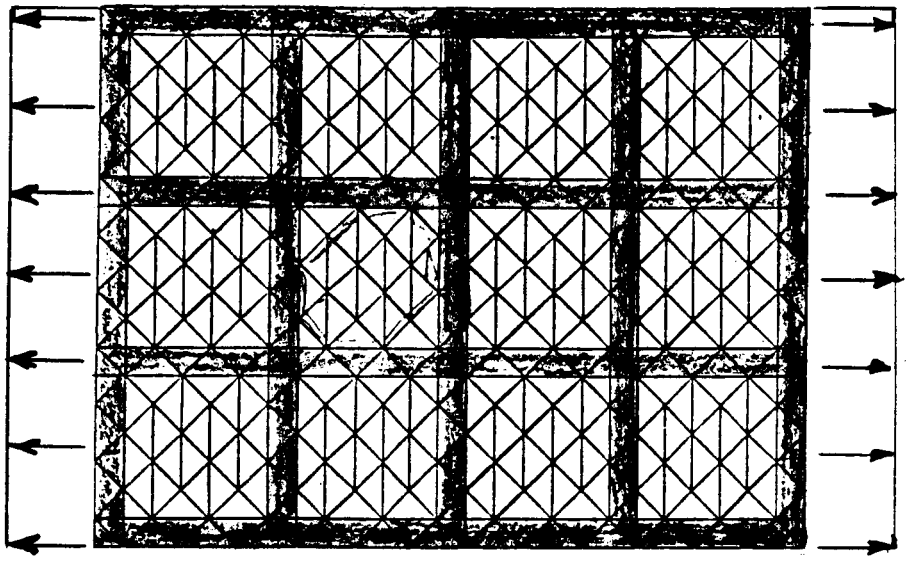

1-a) orthogrid plate

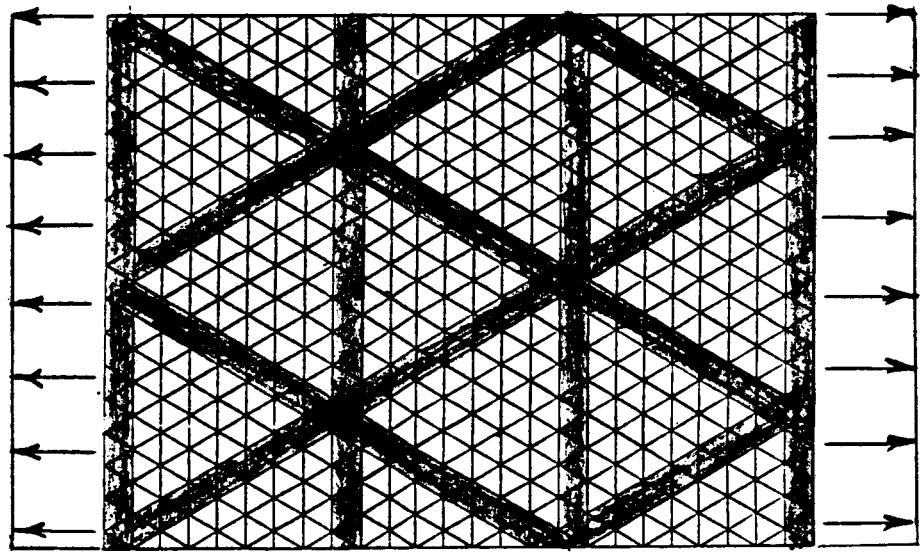

1-b) isogrid plate

Figure 1: Finite element mesh for the orthogrid and isogrid plate configurations.

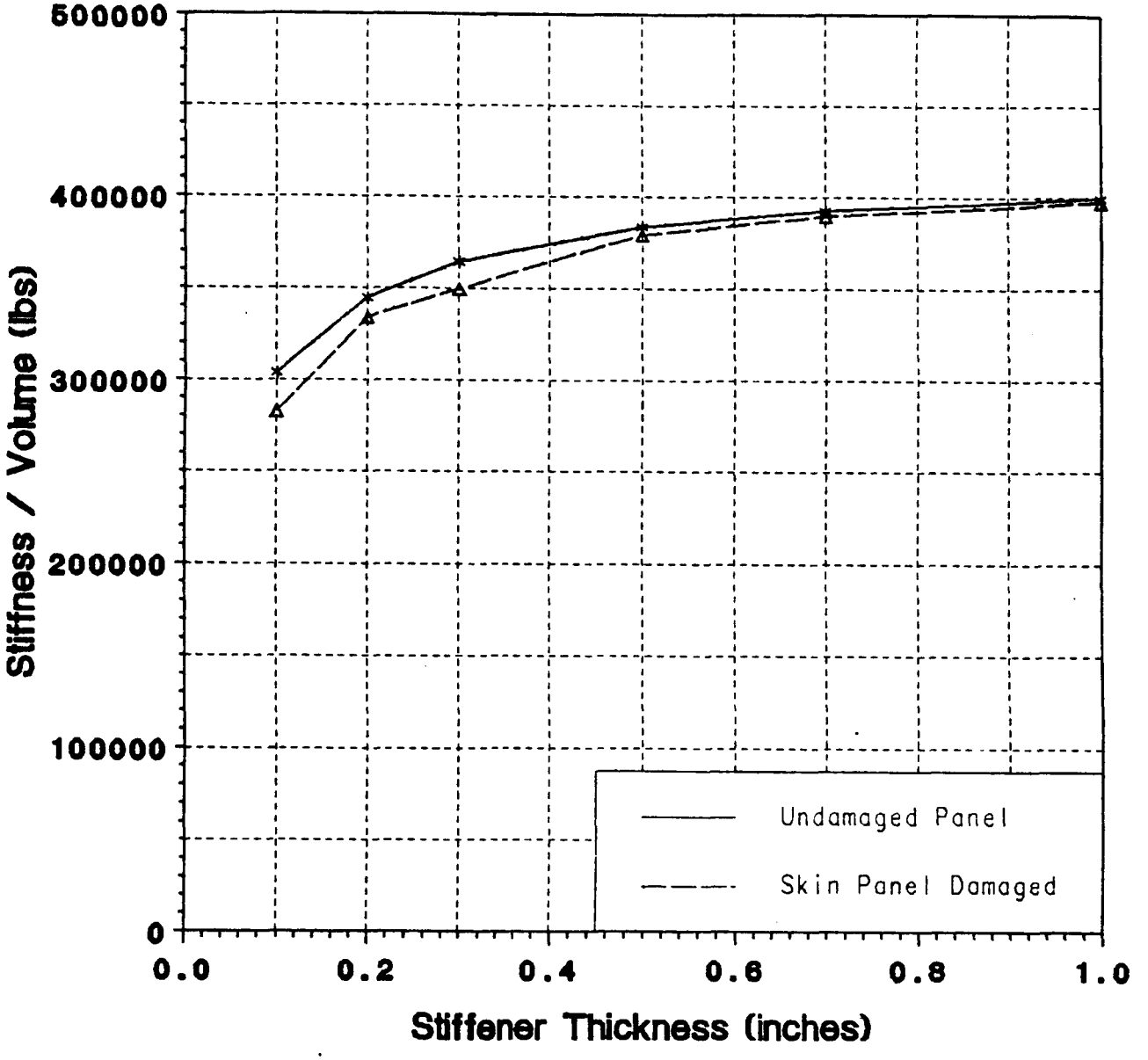

Figure 2: Stiffness of orthogrid plates as a function of stiffener thickness.

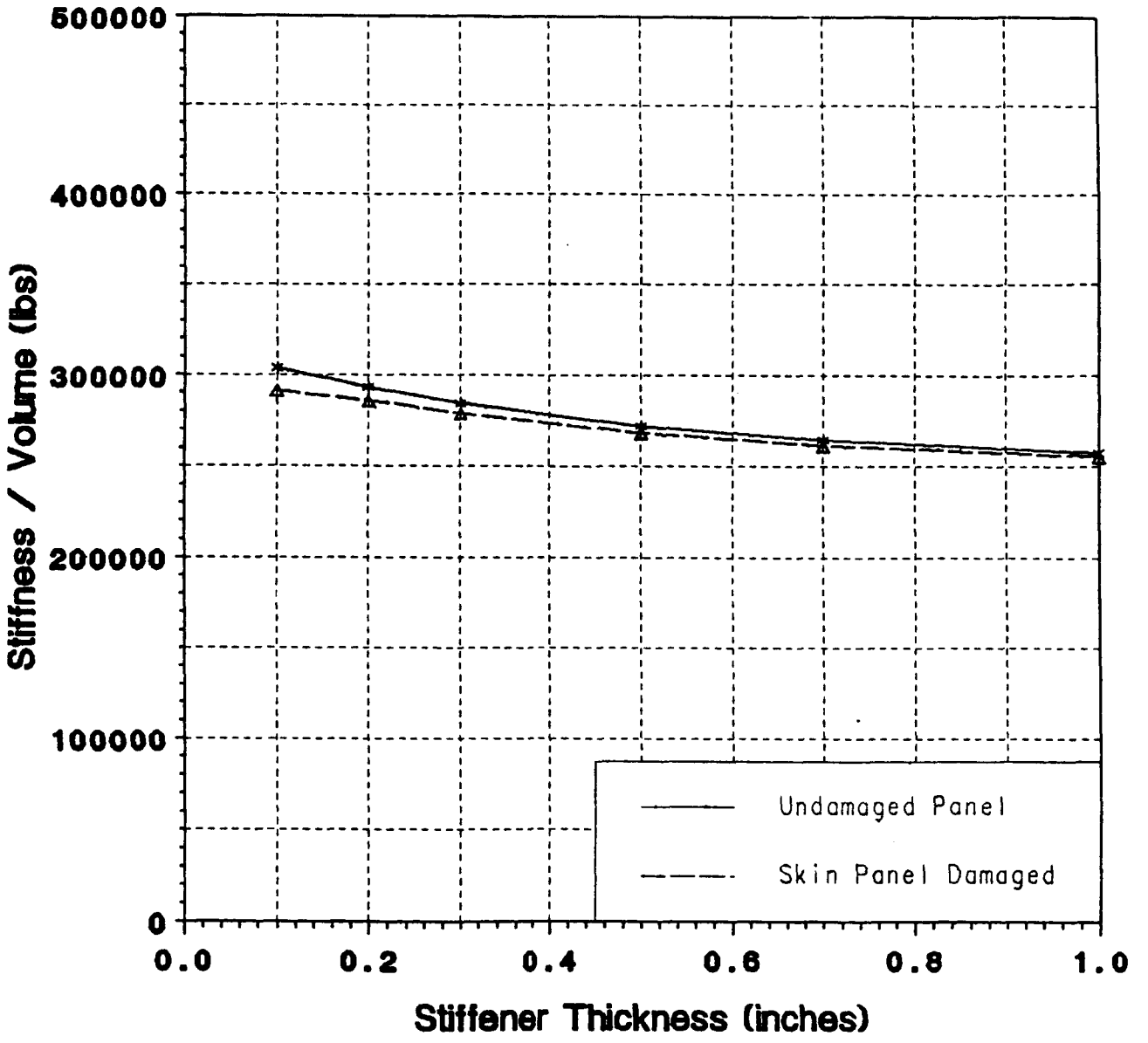

Figure 3: Stiffness of isogrid plates as a function of stiffener thickness.